Original Paper

Finite element modelling of strains and stresses in platinum alloy bushings for textile glass fibre production

Rainer Völkl

Technisches Institut, Friedrich-Schiller-Universität Jena, Jena (Germany)

Bernd Fischer

Fachbereich Werkstofftechnik, Fachhochschule Jena, Jena (Germany)

David Lupton

W. C. Heraeus GmbH & Co. KG, Hanau (Germany)

Roman Teschner

Johns Manville Europe GmbH, Wertheim (Germany)

Platinum components are now very widely used in the manufacture and processing of glass. At first sight it is, therefore, surprising that finite element modelling (FEM) is seldom used in their design. The reason for this omission is to be found in the specific type of mechanical loading at high temperatures and the lack of appropriate mechanical property data for the structural materials. Using the example of a glass fibre bushing from an indirect melt fiberizing process, the paper will demonstrate the use of FEM to determine the stresses resulting from the hydrostatic pressure of the glass melt, the intrinsic weight of the bushing, the stresses caused by the forces applied to withdraw the fibres from the bushing, and the stresses induced by the inhomogeneous temperature distribution in the bushing. On the basis of these model calculations it was possible to localize regions of stress concentrations, to select an appropriate structural material and to modify the component design to reduce the stresses.

Finite Elemente Simulation der Dehnungen und Spannungen in Düsenwannen aus Platinlegierungen zur Herstellung textiler Glasfasern

Platinbauteile werden heute im großen Umfang bei der Herstellung und Bearbeitung von Glas eingesetzt. Auf den ersten Blick ist es darum überraschend, daß die Finite Elemente Simulation (FEM) selten beim Entwurf dieser Platinbauteile zum Einsatz kommt. Als Gründe dafür sind die spezielle mechanische Belastung bei hohen Temperaturen und der Mangel an entsprechenden mechanischen Kennwerten für die Strukturwerkstoffe anzusehen. Am Beispiel einer Düsenwanne für das Indirekt-Schmelzverfahren zur Herstellung von textilen Glasfasern wird aufgezeigt wie FEM benutzt werden kann, um die Spannungen, hervorgerufen durch den hydrostatischen Druck der Glasschmelze, durch das Eigengewicht der Düsenwanne, durch das Abziehen der Glasfasern und durch eine inhomogene Temperaturverteilung in der Düsenwanne, zu ermitteln. Auf der Basis dieser Modellrechnungen konnten Spannungskonzentrationen lokalisiert, ein geeigneter Strukturwerkstoff gewählt und Konstruktionsänderungen zur Spannungsreduzierung aufgezeigt werden.

1. Introduction

Over the last two decades textile glass fibres have gained more and more in importance. The growing variety of applications of textile glass fibres in yarns, twists, fleeces, rovings, glass fibre mats and glass fibres for filters in the chemical industry have led to increasing demands on the production processes. Major progress can only be achieved with improved glass fibre bushings. New bushing technologies should allow longer life cycles and higher glass throughput by means of higher rate of fibre drawing. The use of new precious metal alloys such as Pt-10%Rh DPH from W. C. Heraeus, Hanau (Germany) [1 to 3] is one way to improve glass fibre bushings. Another way to optimize the bushings by means of Finite Element Modelling (FEM) is described in this paper.

Two process types are common for the production of continuous textile glass fibres. In the direct melt process the glass melt flows directly from the tank furnace

Received 12 January, revised manuscript 27 April 2001.

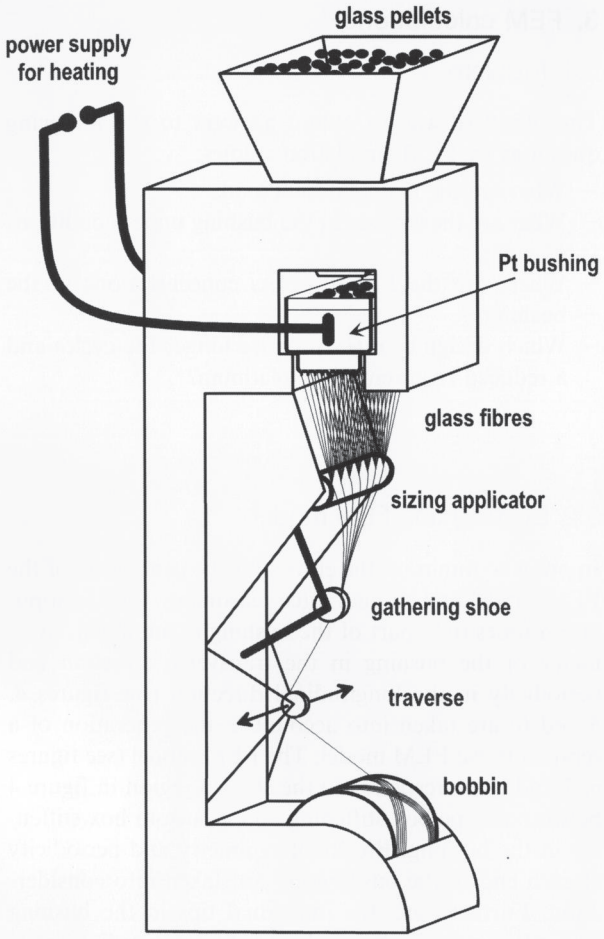

Figure 1. Pt-bushing for production of continuous glass fibres.

through a feeder to the bushing. The indirect melt process consists of two steps. In a first step glass pellets or rods are melted and allowed to solidify. In a second step the pellets are remelted in a bushing. Figure 1 shows a schematic diagram of the indirect melt process applied at Johns Manville Europe, Wertheim (Germany) for the production of textile C-glass fibres and rovings.

The bushing has two purposes. First it should guarantee optimal viscosity of the glass melt for the spinning process. Therefore the bushing is resistance-heated in order to control the temperature distribution within narrow limits. Secondly up to four thousand small nozzles, the so-called tips, are pressed or welded into the base plate of the bushing (figure 2). A glass fibre is withdrawn from every individual tip. The fibre can have a diameter ranging from 5 to 30 µm depending on the tip design and the drawing conditions. Just below the tips the fibres are rapidly cooled and provided with a protective film of size (figure 1).

The material and the design of the bushing are essential factors in the production of high-quality glass fibres. Due to high temperatures of 1200 °C and more together with severe corrosive conditions only platinum alloys can be used for the bushings. The solid solution

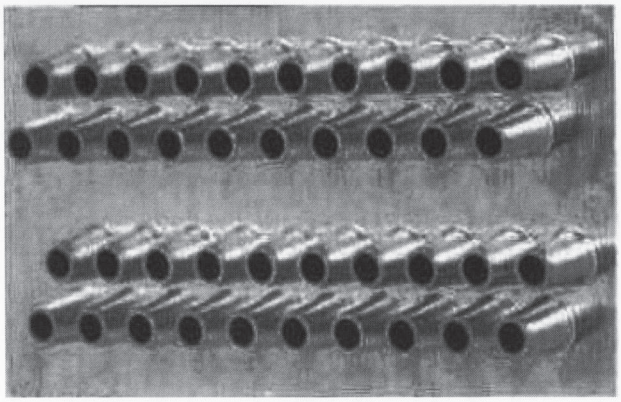

Figure 2. Four tip rows pressed in the base-plate of Pt-bushing for production of continuous glass fibres.

strengthened platinum-rhodium alloys with 10 or 20 % Rh are most commonly used. Oxide dispersion strengthened platinum base alloys were seen as ideal materials for glass fibre bushings but inherent brittleness often prevented glass industry from using them on a larger scale. Recently W. C. Heraeus has introduced a new family of oxide dispersion strengthened platinum alloys, designated DPH materials [1 to 3], which are sufficiently ductile for application in bushings.

At Johns Manville Europe several hundred platinum bushings each weighing about 8 kg are in continuous use. In order to cut costs Johns Manville Europe is undertaking major efforts to use platinum materials more efficiently. High strength alloys such as the DPH materials permit a reduction in the total amount of platinum in a bushing. However, care has to be taken when changing the design because of the double task of heating the melt and maintaining a stable spinning process. Thus a design change cannot be accomplished by the mere reduction of wall thickness in a platinum bushing.

Traditionally, the designs of platinum structures have been improved by trial and error. Some studies [4 and 5] have recently demonstrated the possibilities of FEM. In this paper we describe an approach in which FEM is used in order to simulate the deformation behaviour of platinum bushings. Weak points in the structure could be identified and ways to avoid them will be shown.

2. Material properties

Equipment specially designed at the Fachhochschule Jena [6 to 8] is used for mechanical tests on platinum group alloys and refractory alloys at temperatures up to 3000 °C [9]. The equipment permits creep tests and tensile tests either in air or under inert gas atmosphere. A

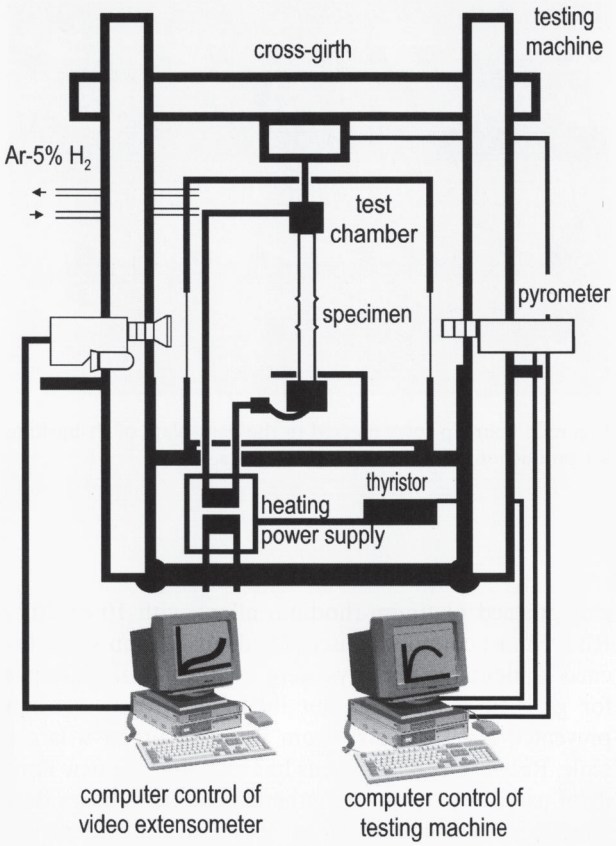

Figure 3. Schematic diagram of the equipment used to measure mechanical properties of metals at temperatures up to 3000 °C.

schematic diagram of the equipment is given in figure 3. The specimen is gripped by clamps and heated directly by an electric current. An infrared pyrometer adjusts the heating current to maintain a constant temperature. The load is applied to the sample by means of calibrated weights. A video extensometer developed in-house [8] continuously determines the strain in the hot-test part of the specimen with an accuracy better than 0.1 %. Mechanical properties of the alloy Pt-10% Rh DPH in the temperature range between 1273 and 1873 K are given in table 1.

3. FEM calculations

3.1 Problem

The objective was to obtain answers to the following questions by FEM simulation studies:

- What are the main external loads?
- What are the stresses in the bushing under conditions of use?
- Where are the highest stress concentrations in the bushing?
- Which design changes promise longer life cycles and a reduced requirement of platinum?

3.2 Bushing and FEM model

In order to minimize the efforts for the generation of the FEM model and to guarantee reasonably short computation times only part of the bushing is simulated. Symmetry of the bushing in the transverse direction and periodicity in the longitudinal direction (see figures 4, 5 and 6) are taken into account in the generation of a representative FEM model. The FEM model (see figures 6, 7 and 8) corresponds to the shaded region in figure 4 between a cope box stiffening and a bottom box stiffening in the bushing. Breaks of symmetry and periodicity at each end of the bushing are not taken into consideration. Furthermore, the individual tips in the bushing base plate and the boreholes in the intermediate plate are also not considered in the FEM model.

The bushing is separated from the steel frame assembly by a ceramic filler compound and an insulating firebrick (see figure 5). In order to protect the bushing from high thermo-mechanical stress due to differential thermal expansion the bearing ensures free slip of the insulating firebrick in the frame assembly. For this reason the FEM model does not incorporate the ceramics (see figures 6, 7 and 8).

For the FEM simulations the commercial software package ANSYS [12] was used. The bushing is made of Pt-10%Rh DPH sheets of various thickness. The thick-

Table 1. Mechanical properties of the alloy Pt-10% Rh DPH in the temperature range between 1273 and 1873 K

parameter	unit	value	source
elastic modulus	MPa	$207 \cdot 10^3 - 48 \cdot T$	[10]
shear modulus	MPa	$94 \cdot 10^3 - 20 \cdot T$	[10]
thermal expansion	1/K	$8.8 \cdot 10^{-6} + 8.3 \cdot 10^{-10} \cdot T$	[11]
0.2 % offset yield strength	MPa	$140 - 0.06 \cdot T$	1)
ultimate tensile strength	MPa	$206 - 0.10 \cdot T$	1)
creep rate	1/s	$3.1 \cdot \sigma^{4.5} \cdot e^{-333\,\mathrm{kJ}/(R\,T)}$	1)

Notes: All stresses in MPa and temperatures in K. Elastic constants and thermal expansion coefficient are for the solid solution alloy Pt-10% Rh.
1) Own measurements.

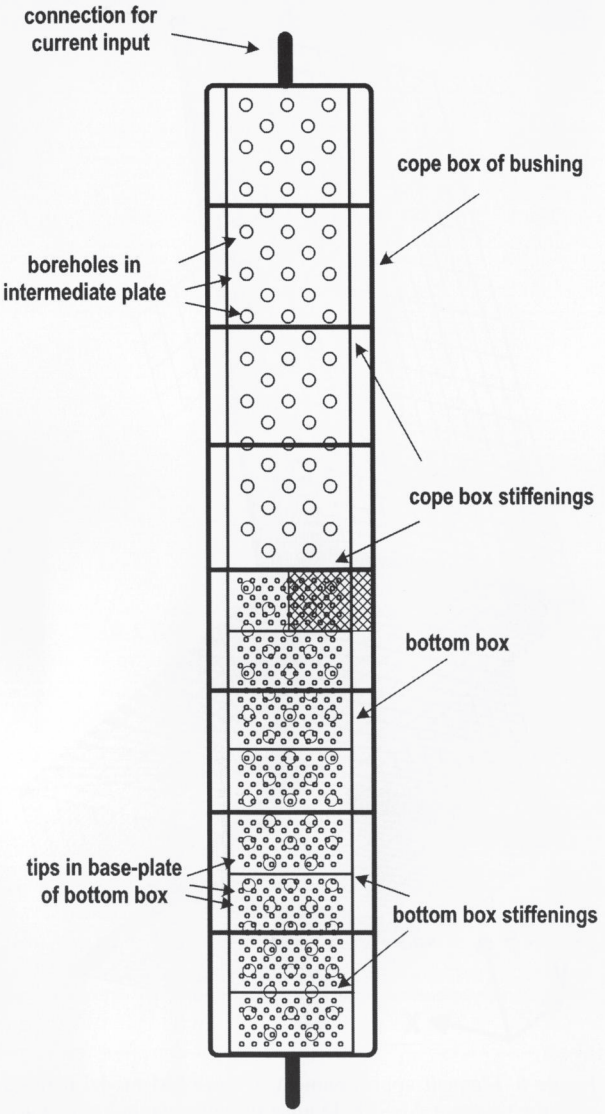

Figure 4. Schematic top view of the bushing without frame assembly and frame support. The shading indicates the region of the FEM model.

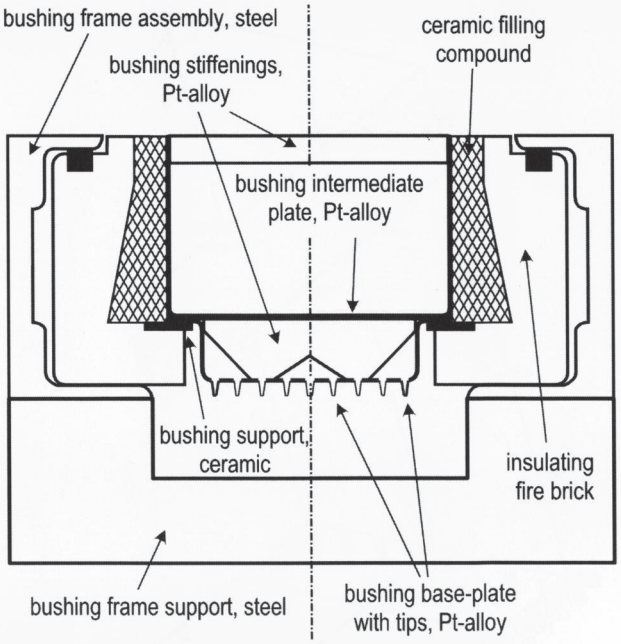

Figure 5. Schematic cross-section of bushing with frame assembly and frame support.

ness of the sheets is fairly small compared to the other two dimensions in space and therefore elastic shell elements are used for the FEM model. The densities of FEM elements are chosen according to the expected stress gradients (figure 7).

An appropriate choice of the boundary conditions is essential for meaningful FEM simulations. Constraints on edge elements reflect the symmetry and the periodicity of the bushing (figures 6, 7 and 8). The outer edge of the intermediate plate may slip freely along the transversal and longitudinal directions but not perpendicular to it. By coupling all degrees of freedom of the edge nodes a stiff weld between bottom box and intermediate plate is simulated (figure 8). The hydrostatic pressure of the glass melt and the fibre elongation forces are simulated by area loads on corresponding areas of the FEM model (figures 6 and 7).

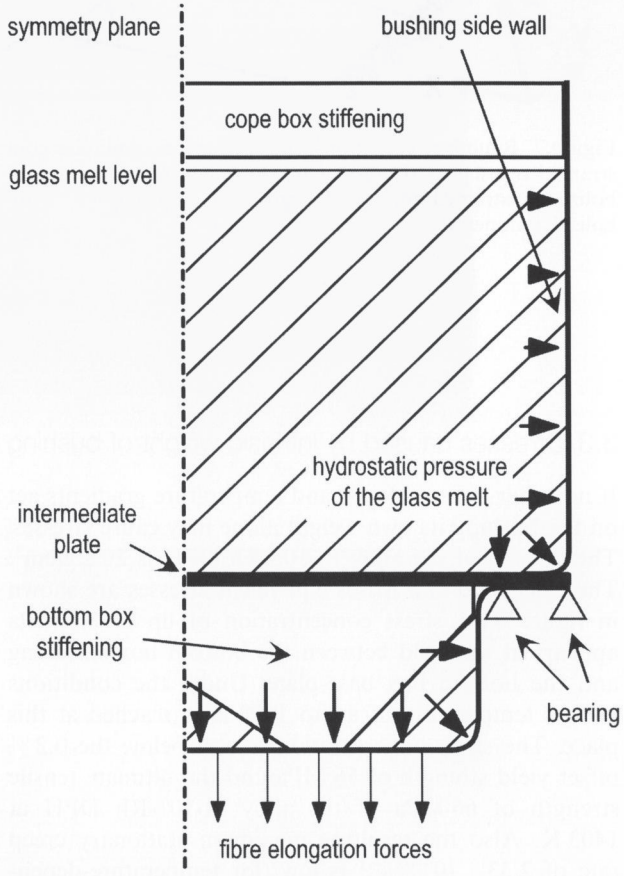

Figure 6. Schematic cross-sectional view of the FEM model of a bushing made of Pt-10% Rh DPH.

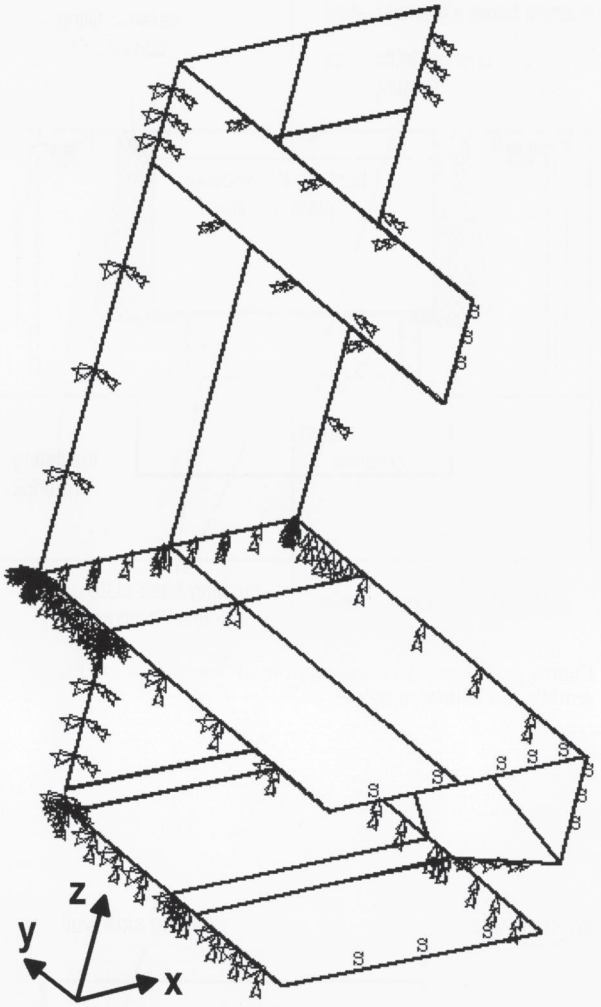

Figure 7. Boundary conditions: single triangles symbolize constrained translatory degrees of freedom, double triangles symbolize constrained rotational degrees of freedom, "S" symbolizes symmetry.

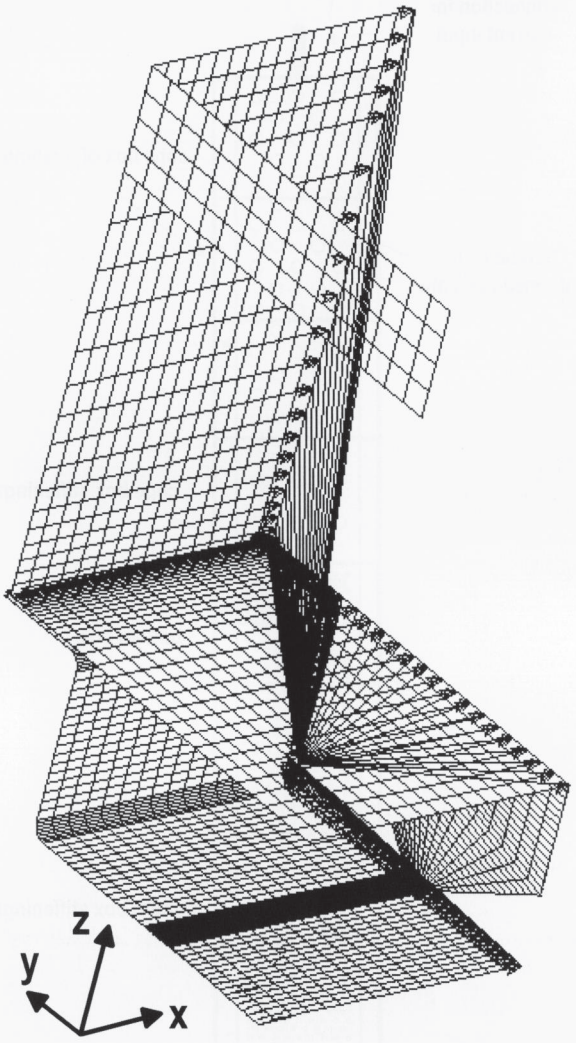

Figure 8. Element apportionment of the FEM model realized with the program ANSYS. Double triangles symbolize coupled degrees of freedom necessary to simulate the periodicity of the bushing and the weld between bottom box and intermediate plate.

3.3 Stresses caused by intrinsic weight of bushing

If no other external loads and temperature gradients act on the bushing its own weight alone may cause stresses. The density of the alloy Pt-10%Rh DPH is 20.2 g/cm^3. The calculated von Mises equivalent stresses are shown in figure 9. A stress concentration of up to 3.2 MPa appears at the weld between the bottom box stiffening and the bottom box base-plate. Under the conditions used a temperature of up to 1403 K is reached at this place. The stress concentration is well below the 0.2 % offset yield strength of 56 MPa and the ultimate tensile strength of 66 MPa of the alloy Pt-10%Rh DPH at 1403 K. Also the resulting maximum stationary creep rate of $2.33 \cdot 10^{-10}\ s^{-1}$ is low (for temperature-dependent material properties of the alloy Pt-10%Rh DPH, see table 1).

3.4 Stresses caused by fibre elongation forces only

Optimal conditions for the spinning process are reached at a viscosity of the glass melt of $\lg \eta = 2.8$. The fibre elongation force on one individual fibre-drawing tip can be approximated by the following expression [13 to 15] and figure 10:

$$F_z = F_\eta + F_\sigma + F_a - F_g;$$

viscous deformation force: $F_\eta = \dfrac{-4\,\eta\,M\,\dfrac{\mathrm{d}R}{\mathrm{d}z}}{\varrho R}$;

surface tension force: $F_\sigma = \pi\,R\,\sigma\cos(\Theta)$;

mass acceleration force: $F_a = M(v_z - v_0)$;

gravitational force: $F_g = \int 2\pi\,\varrho\,g\,R^2\,\mathrm{d}z$;

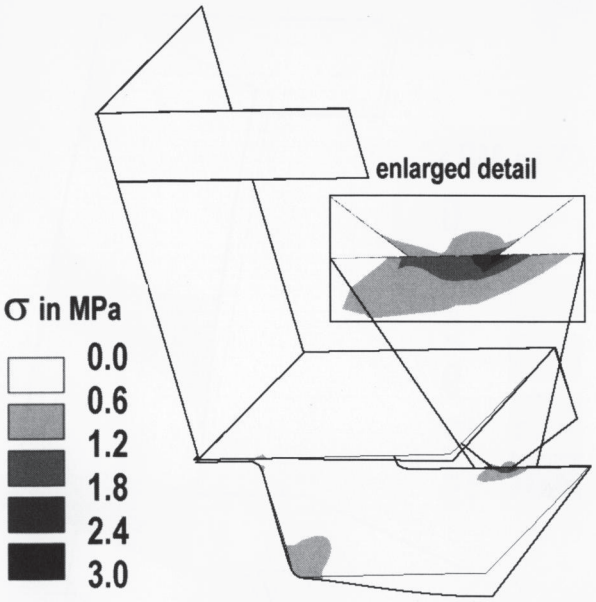

Figure 9. Von Mises equivalent stresses in MPa due to intrinsic weight of the bushing alone. The scaled deformed shape and the undeformed shape are shown.

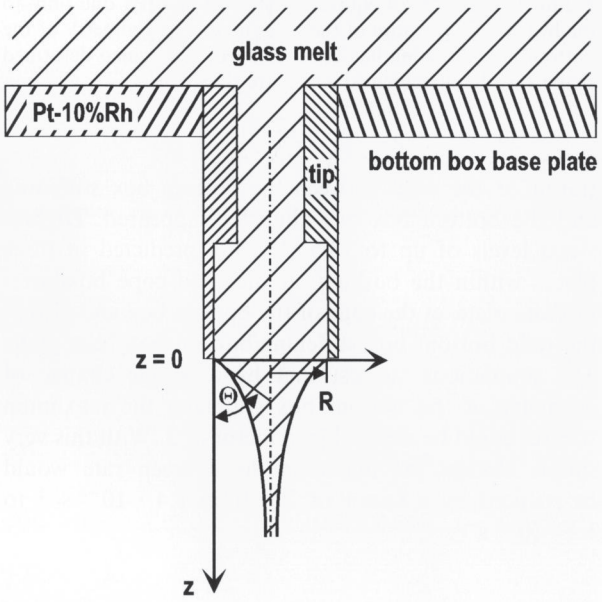

Figure 10. Important parameters for calculation of the forces at an individual fibre-drawing tip [13 to 15].

where R is the radius of the glass meniscus, Θ the angle z-axis/tangent to the glass meniscus, σ the surface tension of the glass melt, M the mass flow, ϱ the density of the glass melt, v_z the drawing velocity at the bobbin, and v_0 the discharge velocity at $z = 0$.

Taking into account the geometry of the tip and the parameters of Johns Manville Europe C-glass the maximum fibre elongation force amounts to $2.73 \cdot 10^{-3}$ N per tip or filament.

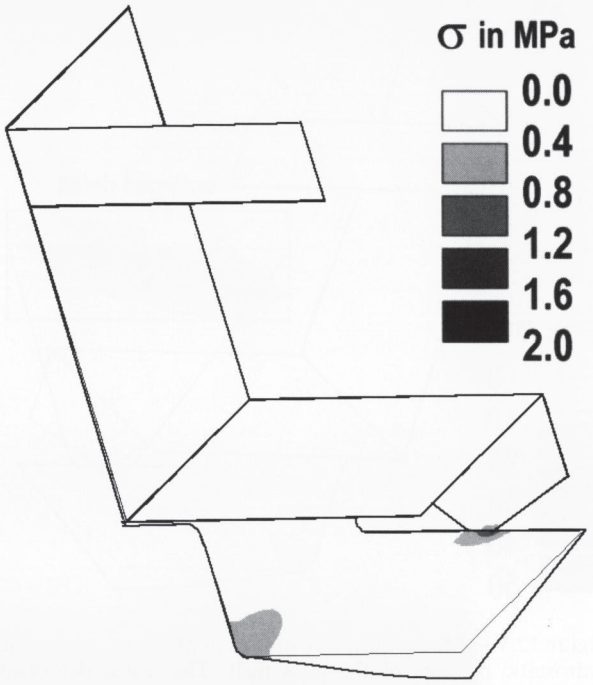

Figure 11. Von Mises equivalent stresses in MPa due only to fibre elongation forces. Drawing of the glass fibres causes the fibre elongation forces. The scaled deformed shape and the undeformed shape are shown.

Von Mises stresses calculated by means of FEM are given in figure 11 for the case where only the fibre elongation forces on the tips act as external loads. A stress concentration of approximately 1.8 MPa is again introduced in the bottom box at the weld stiffening/base plate. The level of the stress concentration is lower than in the above case where only the intrinsic weight of the bushing is considered. The maximum stress is well below the yield strength and the ultimate tensile strength of the alloy Pt-10%Rh DPH at temperatures attained under normal service conditions.

3.5 Stresses caused by hydrostatic pressure of glass melt only

In the production process the level of the glass melt reaches the lower edge of the cope box stiffening (see figure 6). The C-glass melted by Johns Manville Europe has a density of 2.5 g/cm^3. The hydrostatic pressure of the glass melt introduces stresses into the bushing. The most severe stresses concentrate again at the inner welded joint between the bottom box stiffening and the bottom box base plate. At the weld the von Mises stresses of up to 45 MPa almost reach the yield strength (see figure 12). The stress concentration initiates local creep deformation with a high stationary creep rate of $3.4 \cdot 10^{-5}$ s^{-1}.

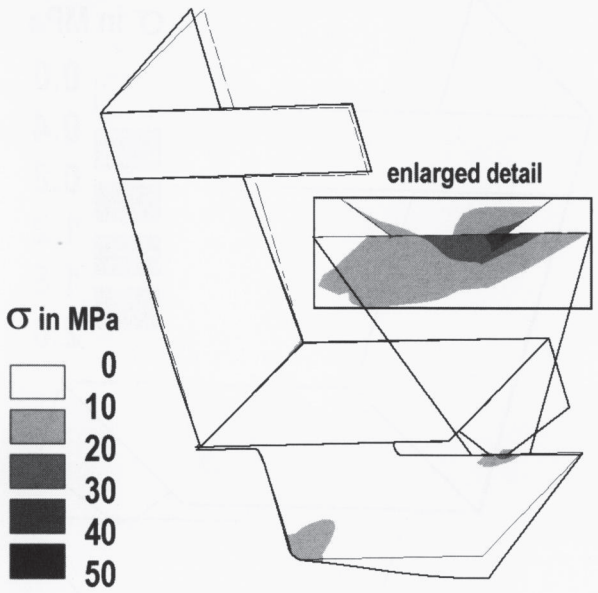

Figure 12.Von Mises equivalent stresses in MPa due only to the hydrostatic pressure of the glass melt. The scaled deformed shape and the undeformed shape are shown.

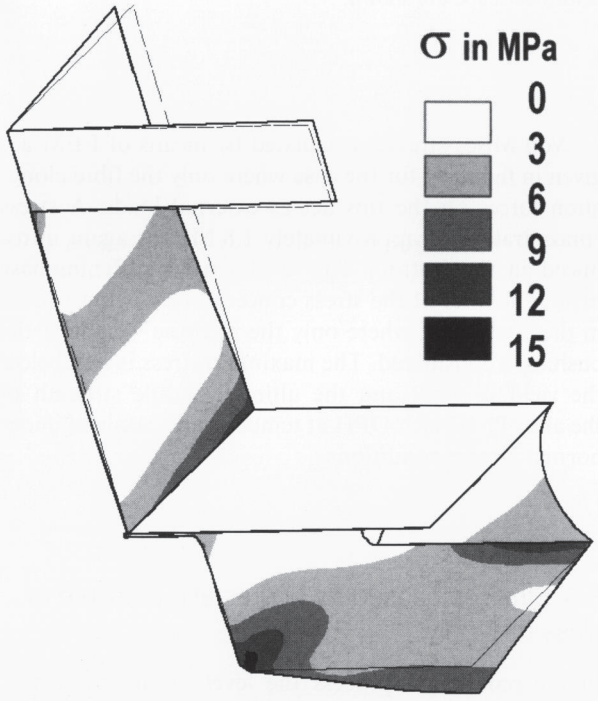

Figure 13. Von Mises equivalent stresses in MPa due only to the hydrostatic pressure of the glass melt. The geometry of the bottom box stiffening has been changed. The scaled deformed shape and the undeformed shape are shown.

In order to overcome this 'weak spot' an alternative geometry is simulated. For the simulations of the von Mises stresses in figures 13 and 14 the geometry of the bottom box stiffening was optimized. The stress concentration at the weld between the bottom box stiffening and the bottom box has almost disappeared. Highest stress levels of up to 13.5 MPa are predicted in three places within the bushing, at the weld cope box/intermediate plate, at the edge of the bottom box and also at the weld bottom box stiffening/bottom box base plate. The simulations suggest that by a simple change of geometry of the bottom box stiffening the maximum stresses could be reduced by a factor of 3. With this very simple change the maximum local creep rate would be reduced by a factor of 200 from $3.4 \cdot 10^{-5}\,s^{-1}$ to $1.5 \cdot 10^{-7}\,s^{-1}$.

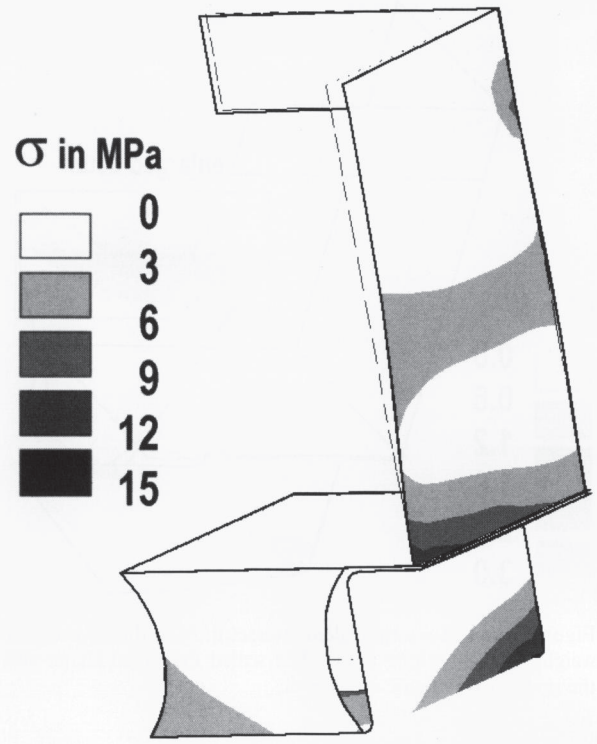

Figure 14. Von Mises equivalent stresses in MPa due only to the hydrostatic pressure of the glass melt. The geometry of the bottom box stiffening has been changed. The scaled deformed shape and the undeformed shape are shown.

3.6 Stresses caused by an inhomogeneous temperature distribution only

The following temperatures were measured in the bushing during normal glass fibre production:

- upper edge of cope box: 873 K;
- intermediate plate: 1483 K;
- bottom box base plate: 1403 K.

For the FEM simulations in figures 15 and 16 constant temperature gradients were assumed both between the upper edge of cope box and the intermediate plate and between the intermediate plate and the lower part of the bottom box.

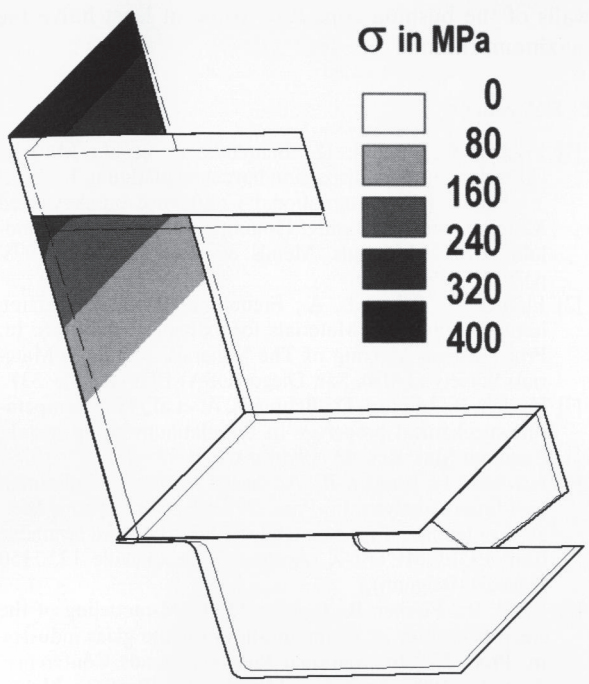

Figure 15. Von Mises equivalent stresses in MPa caused by an inhomogeneous temperature distribution as shown in figure 17. The scaled deformed shape and the undeformed shape are shown.

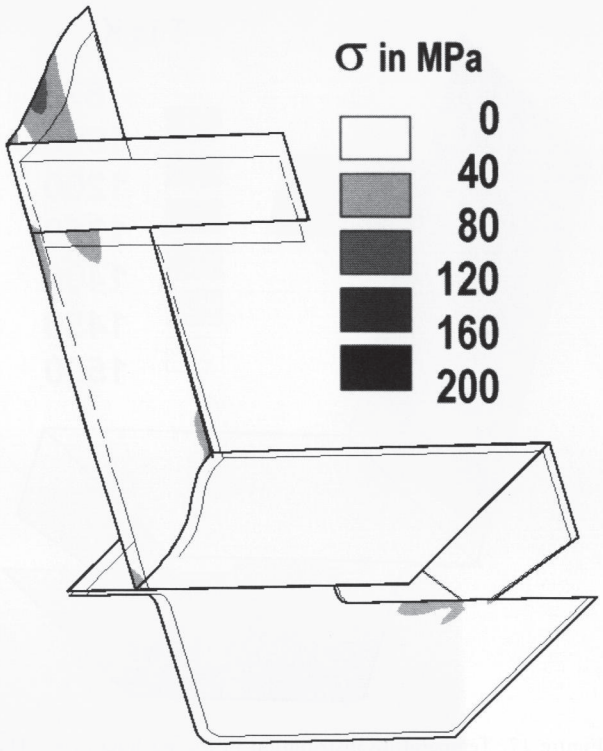

Figure 16. Von Mises equivalent stresses caused by an inhomogeneous temperature distribution as shown in figure 17. The scaled deformed shape and the undeformed shape are shown. In contrast to figure 15 the bushing side-walls have a wave-like shape.

If the inhomogeneous temperature distribution throughout the bushing in figure 17 were attained instantaneously after turning on the electric current, extremely high thermal stresses would be induced. Calculated von Mises stresses of up to 400 MPa (figure 15) would exceed the ultimate tensile strength of the alloy Pt-10%Rh DPH even at the lowest temperature of 873 K at the upper edge of the bushing cope box. This result could be interpreted in such a way that if the temperature rises too rapidly, cracks will occur immediately the bushing is taken into operation. In practice the temperature is increased slowly in order to give the material time to relax thermal stresses by creep deformation. "Creep-brittle" materials, i.e. materials which cannot undergo sufficient creep deformation, might nevertheless form cracks even at low heating rates. Temperature cycling further aggravates this effect because, especially in the case of creep brittle materials, creep deformation is accumulated at every temperature cycle. The previously disappointing experience with the use of brittle conventional oxide dispersion strengthened Pt-alloys in glass fibre bushings can be understood with this interpretation.

Even creep ductile materials can accumulate only a finite amount of creep deformation; therefore the design of the bushing should be optimized in order to reduce thermal stresses. A more favourable geometry is simulated in figure 16. Based on the same temperature distribution as for figures 15 and 17, it was possible to reduce the von Mises stresses considerably. A maximum stress level of 180 MPa is calculated for bushing sidewalls with wave-like shapes.

4. Discussion and conclusions

It is essential to distinguish between loads acting continuously or temporarily. The fibre elongation forces, the load due to the intrinsic weight of the bushing and the hydrostatic pressure of the glass melt act together continuously in the same direction, i.e. they cause stress concentrations at the same points in the bushing design. Among the continuously acting loads the hydrostatic pressure of the glass melt is most important. The weld between the bottom box stiffening and the bottom box baseplate could be identified as a weak point of the present design.

The shape of the stiffening plate should ensure a good initiation of the forces caused by the loads on the bottom box base plate. A bottom box stiffening plate with concave edges would give a much more homogeneous stress distribution (figures 13 and 14). FEM simulations of an alternative geometry have shown that

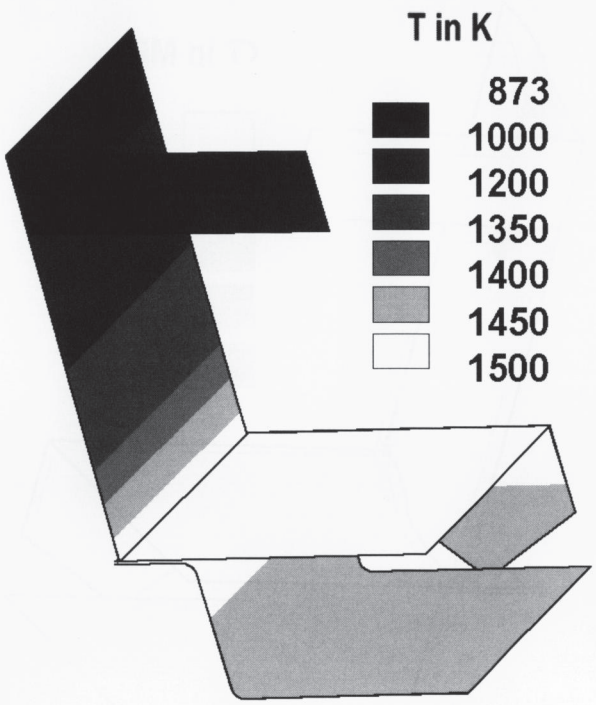

Figure 17. Temperature distribution in the bushing in K. The temperature gradients both between the upper edge of cope box and the intermediate plate and between the intermediate plate and the lower part of the bottom are constant.

with this simple modification the stresses could be reduced by a factor of 3.

Thermal stresses are caused by an inhomogeneous temperature distribution. Care has to be taken when the electric current passing through the bushing is increased on heating the bushing. The temperatures should be increased in such a way that the thermal stresses never exceed the ultimate tensile strength of the material.

Unlike the loads mentioned above the thermal stresses can in principle relax completely by plastic and creep deformation if the material is sufficiently ductile. Thermal stresses vanish with time when the temperature distribution remains stable. However, with any change of temperature distribution plastic and creep deformation is accumulated. Thus, for a long service live of the bushing the thermal stresses should be minimized.

For an optimum spinning process a certain viscosity is needed. For a given glass composition the viscosity at the working point defines the temperature required at the tips. This is the reason why it is not possible to achieve a much more homogeneous temperature distribution in the bushing.

The change in the bushing design is an alternative way to reduce thermal stresses. From the FEM simulations it could be concluded that wave-like shaped sidewalls of the bushing cope box would at least halve the maximum thermal stresses.

5. References

[1] Fischer, B.; Freund, D.; Behrends, A. et al.: Material characterization of dispersion hardened platinum. In: Proc. 3rd Pacific RIM International Conference on Advanced Materials and Processing, Honolulu 1998. Vol. II. Honolulu (USA): Minerals, Metals & Materials Soc., 1998. p. 2951–2956.

[2] Fischer, B.; Behrends, A.; Freund, D. et al.: Dispersion hardened platinum Materials for extreme Conditions. In: Proc. Annual Meeting of The Minerals, Metals & Materials Society (TMS), San Diego (USA) 1999. p. 321–331.

[3] Fischer, B.; Lupton, D.; Behrends, A. et al.: High temperature mechanical properties of the platinum group metals. Platinum Met. Rev. **43** (1999) no. 1, p. 18–28.

[4] Nowicki, T.; Frugier, B.: Advanced methods of platinum part failure analysis. In: Proc. 3rd European Precious Metals Conference, Florence (Italy) 1997. (Offprint available from EUROMETAUX, Avenue de Broqueville 12, 1150 Brussels (Belgium).)

[5] Völkl, R.; Fischer, B.; Gohlke, D.: FEM-modeling of the creep behaviour of platinum alloys for the glass industry. In: Proc. 23rd International Precious Metals Conference, Acapulco 1999. Acapulco (Mexico): Int. Precious Metals Inst., 1999. p. 105–116.

[6] Fischer, B.; Töpfer, H.; Helmich, R.: Anordnung zur Warmfestigkeitsprüfung hochschmelzender, elektrisch leitender Werkstoffe. German pat. DD no. 245 576 A3. Publ. date May 13, 1987.

[7] Fischer, B.; Freund, D.; Lupton, D.: Gerät für Zeitstandversuche bei extrem hohen Prüftemperaturen. In: Proc. Werkstoffprüfung 97, Deutscher Verband für Materialforschung und -prüfung, Bad Nauheim (Germany) 1997. p. 119–125.

[8] Völkl, R.; Freund, D.; Fischer, B. et al.: Berührungslose Dehnungsaufnahme an widerstandsbeheizten Metallzugproben mit Hilfe digitaler Bildverarbeitung bei Prüftemperaturen bis 3000 °C. In: Proc. Werkstoffprüfung 98, Deutscher Verband für Materialforschung- und -prüfung, Bad Nauheim (Germany) 1998. p. 211–218.

[9] Fischer, B.; Freund, D.; Lupton, D.: Stress-rupture strength of rhenium at very high temperatures. In: Proc. Annual Meeting of The Minerals, Metals & Materials Society, Orlando (USA) 1997. p. 311–320.

[10] Lupton, D. F.; Merker, J.; Fischer, B.: Platinum group metals for very high temperature applications. In: Proc. 3rd European Precious Metals Conference, Florence (Italy) 1997. (Offprint available from EUROMETAUX, Avenue de Broqueville 12, 1150 Brussels (Belgium).)

[11] Beck, G. (ed.): Edelmetall-Taschenbuch. Heidelberg: Hüthig, 1995.

[12] Moaveni, S.: Finite element analysis: theory and application with ANSYS. Upper Saddle River, NJ: Prentice Hall, 1999.

[13] Stehle, M.; Brückner, R.: Simultane rheologische und thermische Analyse des Glasfaserziehvorganges. T.1. Numerische Ergebnisse und Vergleich mit den Experimenten. Glastechn. Ber. **52** (1979) no. 5, p. 105–115.

[14] Stehle, M.; Brückner, R.: Grenzen des Glasfaserziehvorganges – Die Einschnür- und Oszillationsgrenze. Glastechn. Ber. **53** (1980), no. 5, p. 130–139.

[15] Pähler, G.; Brückner, R.: Festigkeit von Glasfasern als Funktion der Herstellungsparameter. Glastechn. Ber. **57** (1981) no. 3, p. 52–64.

0501P003

Addresses of the authors:

R. Völkl
Friedrich-Schiller-Universität Jena
Technisches Institut
Löbdergraben 32
D-07743 Jena
E-mail: Rainer.Voelkl@uni-jena.de

B. Fischer
Fachhochschule Jena
Fachbereich Werkstofftechnik
Carl-Zeiss-Promenade 2
D-7745 Jena
E-mail: Bernd.Fischer@fh-jena.de

D. Lupton
W. C. Heraeus GmbH & Co. KG
Engineered Materials Division
Heraeusstraße 12–14
D-63450 Hanau
E-mail: david-lupton@heraeus.com

R. Teschner
Johns Manville Europe GmbH
Faserweg 1
D-97877 Wertheim
E-mail: Roman.Teschner@im.com